JAAS

Accepted Manuscript

This is an *Accepted Manuscript*, which has been through the Royal Society of Chemistry peer review process and has been accepted for publication.

Accepted Manuscripts are published online shortly after acceptance, before technical editing, formatting and proof reading. Using this free service, authors can make their results available to the community, in citable form, before we publish the edited article. We will replace this *Accepted Manuscript* with the edited and formatted *Advance Article* as soon as it is available.

You can find more information about *Accepted Manuscripts* in the Information for Authors.

Please note that technical editing may introduce minor changes to the text and/or graphics, which may alter content. The journal's standard Terms & Conditions and the Ethical guidelines still apply. In no event shall the Royal Society of Chemistry be held responsible for any errors or omissions in this *Accepted Manuscript* or any consequences arising from the use of any information it contains.

ROYAL SOCIETY OF CHEMISTRY

www.rsc.org/jaas

What happens when *n*= 1000? Creating large-*n* geochronological datasets with LA-ICP-MS for geologic investigations

Alex Pullen[1,2], Mauricio Ibáñez-Mejía [1], George E. Gehrels[1], Juan C. Ibáñez-Mejía[3,4], and Mark Pecha[1]

1*Department of Geosciences, University of Arizona, Tucson, Arizona, 85721, USA*
2*Department of Earth & Environmental Sciences University of Rochester, Rochester, New York 14627, USA*
3Department of Astrophysics, American Museum of Natural History, New York, New York 10024, USA
4*Institut für Theoretische Astrophysik, Heidelberg, 69120, Germany*

Abstract

The direct age dating of individual mineral components in sedimentary rocks through the analysis of radiogenic parent and daughter isotopes has been routinely applied to better understand sediment provenance and dispersal patterns for several decades. Time, labor, and financial cost—sadly, not scientific inquiry—are typically the determining factors in the number of analyses run for a sedimentary rock sample during provenance investigations. The number of observations reported for detrital zircon provenance investigations using secondary ion mass spectrometers SIMS and laser-ablation inductively-coupled-plasma mass-spectrometers LA-ICP-MS typically range from *n*= 60–120. In this range, minor, but commonly geological relevant, age components are commonly not identified from the sample aliquot. In addition, the relative proportions of zircon ages from within an age component are typically unreliable for intersample comparisons because the relative proportions of ages from aliquots of *n*= 60–120 may poorly reflect the 'true' proportions of ages from a sample. This study investigates the practicality and usefulness of generating large-*n* (*n*= 300–1000) datasets. A LA-MC-ICP-MS and LA-SC-ICP-MS were used to generate four *n*≈ 1000 datasets. We show that precision large-*n* U-Pb detrital zircon datasets can be created using LA-ICP-MS with total sample-run analysis times that are on par with more traditional studies. At best, most provenance investigations based on *n*= 60–100 have been statistically limited to identifying principle age components. The statistical robustness on *n*= 1000 datasets not only significantly increase the probability that exotic or low abundance age components (i.e., *f*< 0.05) are identified in detrital samples, but it allows for the quantitative comparisons between relatively high abundance age

components in samples. This potentially transformative outcome of large-*n* has the potential to stimulate new avenues of research in sedimentology and tectonics.

1. Introduction

Most detrital mineral studies aim to trace sediment through the rock cycle and/or make inferences about sediment source areas by generating absolute ages or through mineralogical and paleomagnetic proxies (e.g., heavy-minerals, petrography, REE in zircon, and Hf-isotopes in zircon). Absolute age is perhaps the most widely applied method to determine provenance of mineral components in sedimentary rocks, and these serve as a record of protolith ages of rocks from the sediment-source areas. A wide array of radiometric dating techniques have been applied to address provenance and correlations between rock units, for example (U-Th)/He [1]; fission track [2–4], Ar-Ar [5,6], and U-Pb [7–10]. In addition, the absolute age dating of detrital mineral components is also applied to constrain maximum depositional ages, which in some tectonic settings may closely approximate the true age of deposition. The advent of routine geochronological analysis of detrital minerals in sedimentary rocks has not only been crucial for chronostratigraphic purposes, but also for resolving regional tectonic and crustal evolution questions. Although the numbers of systems and applications are vast, U-Pb in detrital zircon stands out as the most widely applied geochronologic tool for sedimentary provenance [7–10], with hundreds of articles published every year over the past decade.

Zircon ($ZrSiO_4$) has typically been the mineral of choice because it is resistant to chemical and mechanical weathering, and remains a geochemically closed system through nearly all surface/crustal processes [9]. Zircon commonly has high U concentration (100–1000 μg/g), tends to exclude Pb during crystallization (ng/g), is a common accessory mineral in intermediate–felsic rocks, is abundant in clastic sedimentary rocks, and retains Pb and U at geologically high temperatures ($T_c \approx 900°$ C)[11,12]. These features make zircon ideally suited for being used as a geochronologic provenance indicator. In addition, Pb/U measurements can be made with a range of analytical techniques [13].

Recognizing the application of U-Pb zircon geochronology as a powerful tool to address a wide range of problems in the Earth sciences, an intense effort has been made in the past four decades to improve the accuracy and ease with which these measurements can be made. Datasets created with isotope dilution thermal ionization mass spectrometry (ID-TIMS) have commonly been small (e.g., n= 10–30) because of the time intensive process. ID-TIMS detrital zircon studies have been statistically inadequate to address many of the problems that workers have sought to address (Fig. 1). Secondary ionization mass spectrometer (SIMS) datasets have larger but still limited (e.g., n= 20–60), whereas previous LA-ICP-MS datasets have been even larger (e.g., n= 60–117), but still not sufficient to fully characterize low abundance age fractions within a given sample (Fig. 1) [14].

Some precision is sacrificed with ion probes and LA-ICP-MS as opposed to ID-TIMS [15,16]. Precision for SIMS and LA-ICP-MS are typically reported in the range of ±1–2% [17], whereas ID-TIMS can be better than ±0.1% for individual analyses [13, 18].

This study is an attempt to develop methodologies for LA-ICP-MS analysis of detrital zircons that allow for generation of larger and more robust data sets without significantly increasing the analysis time or compromising analytical precision or accuracy. We report a suite of LA-ICP-MS U-Pb zircon age measurements conducted with a modified routine that allows for obtaining ages with 3–9 s of ablation time and 6–14 s of total analysis time (Table 1). With all analysis requirements considered (e.g., baseline measurement, washout time, and the rate at which the laser can move between crystals) approximately ~180 analyses can be completed per hour. Short acquisition times hold a tremendous advantage for most detrital mineral studies and results in more statistically robust datasets [19–23].

Statistical robustness is invaluable for geochronologic provenance investigations and for making correlations between samples, stratigraphic sequences, and terranes. Loosely defined for provenance studies, statistical robustness implies that every relevant mineral age fraction present in a specific sample is identified from the concentrated zircon aliquots. The probability of not failing to identify an age fraction present in a sample from an aliquot increases as n increases [10, 14, 20]. Failure to characterize each

relevant age component in a sample has the potential for misguided and inaccurate geologic interpretations.

Since the first publication of U-Pb detrital zircon ages using LA-ICP-MS methods [21], huge advancements in lasers and ICP-source mass spectrometers over the last two decades has allowed for individual analysis time and uncertainties to decrease. A major improvement in the LA-ICP-MS analysis time has come as laboratories have started generating detrital zircon ages using integrated total counts of Pb and U rather than a series of integrated Pb/U ratios which require longer counting times [23–25]. Motivated by greater efficiency and the need for more statistically robust datasets, we present large observation (n= 300–1000, herein referred to as large-n) U-Pb detrital zircon data generated by LA-MC-ICP-MS and LA-SC-ICP-MS at the Arizona LaserChron Center, University of Arizona. Through this enhanced efficiency we argue that most detrital zircon provenance studies, and possibly some studies only concerned with constraining maximum depositional age, would benefit from the enhanced statistical certainty of large-n investigations. Additional refinements in sample preparation, imaging, and automation of LA-ICP-MS acquisitions make large-n practical and cost effective for most geochronologic U-Pb detrital mineral investigations.

2. U-Th-Pb Detrital Zircon Provenance

One aim in U-Pb detrital zircon provenance investigations is to identify each age present in a sample and relate that age to a proto- and/or intermediate source(s) to better understand sediment dispersion patterns and guide geologic interpretations. Detrital zircon provenance relies on the assumed random sampling and age generation of zircon crystals separated from sedimentary rocks. Biases introduced during field sampling, mineral separation, mounting, and analysis could result in an incomplete (or biased) distribution of ages used for provenance and thus for intersample comparisons. U-Pb zircon age distributions are influenced by grain-size distribution [26], therefore care must be taken to maintain random grain-sizes across mounts by means of a premixed pour onto mounting tape prior to

epoxy. Additional fractionation can be introduced during magnetic separation during sample preparation [27].

3. The Adequacy of *n*

A problem arises when trying to determine the number of observations (*n*) for a given detrital sample in order to accurately model provenance because the number of age fractions in a sample is unknown before it is analyzed, and possibly after if an insufficient number of observations are taken. The number of age fractions in a given sample can be estimated in advance based on the geologic context of the sample. This estimate can then be used to guide research (e.g., ref. 28). For example, the number of expected age fractions for a sample from a volcanic basin near its perceived sedimentary source would be low, perhaps limited to only one age fraction, whereas the number of age fractions from a river delta at the terminus of a continent-scale river (e.g., Mississippi, Yangtze) would be much higher [29,30].

The question of statistical adequacy of *n* in detrital provenance studies is contentious. As implied above, the number of observations needed for adequacy scales differs with differing numbers of age fractions. The likelihood of missing age fractions and thus yielding an incomplete picture of the age components within a sedimentary rock sample has been expressed as (Eg. 1):

$$\boldsymbol{P = (1 - f)^n}$$

with probability (*P*) that an age fraction is not identified if *n* number of crystals are analyzed for a given proportion of the total number of age fractions (*f*) within a sample [20]. From this, previous workers have concluded that 60 analyses must be completed in order to reduce the probability of failing to identify an age component at a fraction of 1 in 20 ($f = 0.05$) to $P < 5\%$ [9, 20, 28]. This approach is adequate in the scenario that there is only one particular age provenance component of interest. However, Vermeesch [14] noted that, in general, provenance studies are interested in identifying all relevant age components. To that end, Vermeesch [14] argued that a binomial probability model would be more robust for determining statistical

adequacy for uniform population data sets where the number of age components is >1. This work noted that there would be a 64% probability that at least one fraction ($f \geq 0.05$) in a sample with 20 uniform components would be missed when $n = 60$. Rather, it was argued that 117 analyses would be required to reach a 5% probability that no fraction greater than 1 in 20 would be missed. Monte Carlo simulations demonstrate that the rate of failure to identify a low abundance fraction like $f \geq 0.05$ diminishes to less than ~1% for $n > 300$ [10].

As an acknowledgement of the accuracy and precision limitations of SIMS and LA-ICP-MS in the context of the U-Pb system, any given age fractions should ideally be identified more than once within a sample in order for that age fraction to be considered a geologically meaningful result. The approach to numerous provenance studies suggests that every date determined for a detrital sample is geologically accurate and relevant (e.g., ref. 8). However, this may not always be the case. Although discordant ages can reflect geologically significant events, they can lead to misguided interpretations because the cogenetic nature of zircon crystals yielding similarly discordant ages in a detrital sample is uncertain. A balance is typically struck in U-Pb detrital zircon studies between percent discordance and inclusion as a data point [15]; the discordance threshold for inclusion is usually placed at 20–30% [31]. Evaluating a small degree of Pb-loss or inheritance can be challenging given the precision of most U-Pb zircon analyses with SIMS and LA-ICP-MS [32–34], especially for younger ages where the measurement of ^{207}Pb becomes more uncertain. However, any number of important geological interpretations could hinge on a particular age fraction within a detrital sample. The problem of Pb-loss is more precarious for provenance studies of metasedimentary rocks because of the increased likelihood of postdepositional Pb-loss and the possibility that the youngest age fraction, reflecting Pb-loss, is younger than the depositional age of the rock. For these reasons, we agree with the interpretations of Dickinson and Gehrels [35] and suggest that age-based provenance and correlation interpretations of LA-ICP-MS data are more reliable when populations are made with age fractions of $n \geq 3$. This reduces the likelihood of misinterpreting an otherwise, geologically speaking, irrelevant age fraction of $n = 1$ as something meaningful.

Single LA-ICP-MS ages are, by themselves, typically not geologically meaningful as the accuracy of a single U-Pb zircon age analysis can be poor irrespective of precision. U-Pb zircon crystallization ages for noncomplex igneous rocks generated with SIMS or LA-ICP-MS are generally reported as a weighted mean of an interpretably cogenetic cluster of ages. Following this logic, if the $n \geq 3$ threshold is applied, much larger numbers of observations are needed in detrital provenance studies than are traditionally applied to have confidence that determined ages hold 'true' geological significance.

The application of large-*n* datasets in geologic investigations will increase the probability that low abundance fractions are identified, and that age abundances generated from sample aliquots will more closely match the 'true' age abundances of the rock unit being investigated. The identification of low abundance age fractions are especially important in certain scenarios like determining the maximum depositional age of a unit, or first or last appearance of an exotic component within a stratigraphic succession. As *n* increases the measured age distribution should approach the true age distribution, so long as there are no significant biases in sample preparation, grain selection, and data processing/filtering. This has profound implications for studies where relative age fraction abundances, especially of small fractions are important. Determination of unroofing histories archived from foreland basin sediments or inferring erosions rates are two examples where observed age abundances less skewed from the 'true' abundances may result in more accurate geologic interpretations (e.g., ref. 36 and 37).

4. Methods

The four trials of large-*n* U-Pb isotopic analyses reported here where collected using a Photon Machines Analyte-G2 ArF 193 nm Excimer laser-ablation system with HelEx sample cell coupled to: 1) Nu Plasma HR multi-collector MC-ICP-MS (Trials 1 and 2; Table 1); and 2) Thermo Element2 single-collector SC-ICP-MS (Trials 3 and 4; Table 1). For internal consistency, all trials were conducted on a single sample, CP40, a fluvial quartz arenite unit capping the Upper Cretaceous Wahweap Formation on Hernieville Creek, Utah, previously reported in Dickinson and Gehrels [38]. This sample was selected because it contains a wide distribution of ages and proportions of age groups. Trials 1, 2, and 3 where all

completed on different grain mounts of the CP40 sample. Trial 4 consisted of reanalysis of the grain mounts used in Trials 1 and 2 with 500 analyses per mount. The analyses were conducted *in-situ* by laser ablation of epoxy grain mounts. Zircon was separated from the sandstone using a Wilfley Table, methylene iodide, and Frantz magnetic separator following Gehrels et al. [15, 39, 40] and Dickinson and Gehrels [38]. Each step in the mineral separation process has the potential to preferentially remove an age population from a sample thus biasing the outcome of the experiment [41]. However, mineral separation is a necessary part of most U-Pb detrital zircon provenance investigation because of the need to analyze large numbers of crystals (typically from grain mounts). The introduction of mineral separation induced biases can be minimized during the separation process [27].

Fragments of a megacrystic Sri Lanka zircon ($^{206}Pb/^{238}U$ age= 563.5 ±2.3 Ma 2σ [15]) were mounted along with aliquots of CP40 and analyzed in standard-sample bracketing (1:5) to correct for Pb/U isotope fractionation and determine approximate elemental concentrations of U and Th. Additional crystals of known age, R33 ($^{206}Pb/^{238}U$ age= 419.3 ±0.4 Ma 2σ [42] and 420.53 ±0.16 Ma 2σ [43]), were used as a secondary reference material and were treated as zircon crystals of unknown age along with crystals from CP40 in order to independently assess the accuracy of the fractionation corrections. Following SEM imaging of the grain mount, but before laser ablation, the mounts where placed in an ultrasonic bath of 1% HNO3+1% HCl for 10 minutes to remove contamination from the sample surface. In addition, a pre-ablation cleaning pass of 3 bursts was made with the laser prior to data acquisition (Table 1).

In order to test the accuracy of U-Pb zircon ages generated using a total counts data-reduction method with LA-MC-ICP-MS and LA-SC-ICP-MC, zircon crystals with published TIMS ages were analyzed using the methods outlined in Table 1. Offsets between ID-TIMS and our LA-ICP-MS ages are small; most U-Pb ages generated by LA-SC-ICP-MS total counts are within ±1% (2σ) of the published $^{206}Pb/^{207}Pb$ and $^{206}Pb/^{238}U$ ages, whereas ages generated with by LA-MC-ICP-MS range from ±0–2.5% (2σ; Fig. 2). The difference is mainly due to the smaller spot size used for the MC-ICP-MS analyses

Targeting of grains for analysis was conducted both online and offline. Online targeting was conducted using the live video feed from the Photon Machines laser along with a high-resolution BSE

image resolved to show zircon growth zonation (Trials 1, 2, and 4). This technique is less efficient as it requires the mass spectrometer to remain idle while points are being selected in the laser ablation system. The alternative, offline targeting, is based on a high-resolution composite BSE image that has low-distortion. The low-distortion composite image is imported into the Photon Machines Offline Targeting program, points are selected offline, coordinates are exported as a .csv file, and then the points are re-coordinated with the mount based on its position within the HelEx cell just prior to U-Pb analyses. Offline targeting of analysis points is more efficient because spot selection can be completed offline while the laser ablation system and mass spectrometer are used for other projects. The offline targeting approach increases the practicality of acquiring large-*n* datasets and allow mass spectrometers to be operated more efficiently [49].

Data reduction was handled using AgeCalc, an in-house Excel®-based Visual Basic data reduction macro [15]. AgeCalc handles: Pb/U fractionation corrections; initial-Pb correction; calculating and propagating errors; and assigning high initial-Pb, discordance, and reverse discordance filters. The total-count acquisition routine on the Nu Plasma MC-ICP-MS follows that of Johnston et al. [25], whereas the total-count acquisition routine for the Element2 is discussed below and outlined in Table 1.

In the case of SC-ICP-MS, where masses are not measured simultaneously, dwell times on each mass need to be optimized in order to account for the differing relative abundances when uncertainties are to be calculated based on counting statistics. Errors reported for the Element2 analyses (Trials 3 and 4) in the repository datatable are quoted with three levels of uncertainty, which are briefly explained below.

Each measurement cycle on the Element2 was scaled with respect to the dwell-time on each mass in order to calculate the effective number of ion impacts seen by the detector during the sample time. From that it follows that the total number of counts for each isotope TC*i* during a number of cycles *n*, is calculated as the total sum of the counts that were effectively seen by the detector during each measurement pass (Eq. 2):

$$TC_i = \sum_{cycle=1}^{n} \frac{cps_i}{dwelltime_i}$$

Uncertainties for each of the individual isotope measurements were estimated from Poisson counting statistics as the square root of the total counts of each isotope *i* (Eq. 3),

$$\sigma_{meas}(i) = \sqrt{TC_i}$$

Uncertainties for each isotope ratio were propagated following Eq. 4:

$$\sigma_{meas}\left(\frac{i_1}{i_2}\right) = \left(\frac{i_1}{i_2}\right) * \sqrt{\left[\frac{\sigma(i_1)}{i_1}\right]^2 + \left[\frac{\sigma(i_2)}{i_2}\right]^2}$$

The value of $\sigma_{meas}\left(\frac{i_1}{i_2}\right)$ is the first level of uncertainty reported in the apparent ages of the data repository. As discussed by Cottle et al. [23] and the PlasmAge network (www.plasmage.org), the minimum uncertainty of any given measurement should incorporate the calculated uncertainty for that measurement and the excess variability observed on the primary reference material (i.e., Sri Lanka zircon in this case). For each one of the analytical sessions, we derived a normalization uncertainty factor (or overdisperssion factor, ε) required in order to make the MSWD of the reference material equal to 1. This excess scatter was then propagated in quadrature with the calculated uncertainty of each data point in order to obtain the minimum uncertainty of each individual measurement as follows (Eq. 5):

$$\sigma_{min}\left(\frac{i_1}{i_2}\right) = \sqrt{\varepsilon^2 + \left[\sigma_{meas}\left(\frac{i_1}{i_2}\right)\right]^2}$$

This procedure was followed for calculating the reported uncertainties for both the $^{206}Pb/^{238}U$ and $^{206}Pb/^{207}Pb$ values, and is the second level of uncertainty quoted in the reported apparent ages. This is also

the level of uncertainty used to plot the concordia diagrams and calculate the ages of the secondary standards shown in Figure 2.

As a final step, the systematic uncertainties associated with the calibration of the primary reference material, uranium decay constants, and common-Pb composition were propagated. The result of this is the third level of uncertainty in the apparent ages.

4. Large-*n* Results

In general, the reproducibility of a measured age distribution improves with increasing *n*. The distribution of ages from Trials 1–4 in cumulative probability plots show that the misfit of cumulative probabilities between aliquots of the same sample is smaller for $n \approx 1000$ (Fig. 3A) than $n = 100$ (Fig. 3B). This observation suggests that the observed distribution of ages for Trials 1–4 may more closely approximate the 'true' distribution of zircon ages from sample CP40 with all other things being equal (e.g., representative sampling). When Trial 1 is divided in 10 parts of $n = 100$—chosen here for comparison because most SIMS and LA-ICP-MS U-Pb zircon provenance studies do not exceed 100 analyses per sample—a wider range in cumulative probabilities is observed (Fig. 3B). This suggests that although more traditional U-Pb zircon provenance studies (i.e., $n = 100$) may identify zircon ages from low abundance age fractions ($f = 0.02$–0.05), they poorly predict the 'true' abundance of ages in a sample. The likelihood that the observed proportion of ages deviates from the 'true' proportion increases with decreasing n [10] (Fig. 3C). Not surprisingly, the largest divergence in cumulative probability of Trials 1–4 is observed in age ranges that contain zircon ages in low abundance, whereas the cumulative probability of ages in the high abundance ranges (e.g., 1000–1300 Ma) are nearly indistinguishable. The latter observation suggests that the number (of high abundance) ages in large-*n* samples may be quantitatively compared between samples. This observation is important as most previous detrital zircon provenance investigations ($n \leq 100$) have only been statistically sufficient to focus on the presence or absence of an age fraction (Fig. 4). Large-*n* will allow workers to base sound geological arguments on the comparisons between relative proportions of detrital ages in samples.

The ideal means to visually represent, compare, and discuss detrital zircon age data is widely debated. Most previous workers have used univariant probability density plots (PDP) to scrutinize the results of detrital age spectra, an approach recently challenged by Vermeesch [50,51], who postulated Kernel Density Estimations (KDE) as a more statistically sound alternative. PDP are visually descriptive representations of ages and uncertainties of those ages from a sample. KDE can be considered a statistical means of extracting the predictive information contained within a PDP. Figure 4 shows the univariant plots using PDP, KDE, and histogram plots, constructed using the in-house Python® code *DensityDist* and incorporating a Gaussian Kernel density function. Arguably each one of these visual/statistical comparisons has its own strengths and/or might be more adequate to use depending on the question being pursued with the analyses. The KDE function considerably oversmooths the distribution in the young portion of the spectrum when n= 100, whereas the young portion of the spectrum is better captured by the PDP (Fig. 4A). This oversmoothing is made evident by comparing these subsets of n= 100 (Fig. 4A) with their parent distribution represented by Trial 1 (n= 1029; Fig. 4B) or all four Trials combined (n= 4116; Fig. 4C). This tendency of KDE to oversmooth low density areas of the age spectrum may be improved by incorporating adaptive kernel functions that better optimize the bandwidth for the local data density across the age spectrum, or by considerably increasing the number of observations (as bandwidth is inversely proportional to n). Figures 4B and 4C show that the second option is a feasible alternative, and that for large values of n the density curves obtained using PDP and KDE functions effectively converge. The large-n examples also nicely show that, as predicted by Vermeesch [50], the PDP can oversmooth the density distribution for the old portion of the age spectrum when compared to the KDE as a result of increased analytical uncertainty. Based on these observations we suggest that plotting PDP, KDE, and histograms together may help investigators interpret and discuss detrital zircon age results.

The geochronological analysis of detrital-zircons in sedimentary rocks does not always only seek to answer a single particular question (i.e. identify each age fraction present by statistically approximating the parent distribution of ages in a given sample). Many workers use detrital zircon geochronology as a means to obtain a maximum depositional age and thus place constraints on the depositional age for the

sediments in question (e.g., refs 35 and 52). In this context each dated grain constitutes an independent geological observation provided that all sources of analytical uncertainty are appropriately accounted for. It was shown by Dickinson and Gehrels [35] that maximum depositional ages can be reasonably approximated from a weighted-mean of the youngest overlapping population. However, caution must be taken will applying this approach to constrain depositional ages. In many circumstances such as post-depositional Pb-loss [53], thermal overprinting [54], and wide gaps between source terrane age and 'true' depositional age may lead to abuse of 'maximum depositional ages' to alter regional depositional ages, terrane boundaries, or possibly infer nonexistent structures. Large-*n* analyses considerably increase the probability that the youngest grains in a sample will be analyzed. Once the grains that form this youngest population have been identified, the researcher would be able to isolate them for further higher-precision analysis (e.g., ID-TIMS) if desired.

Recognizing that Trials 1–4 with $n \approx 1000$ aliquots may reasonably approximate the 'true' abundances of ages in CP40, but will never fully resolve it, is important. The true age distribution cannot be known unless all zircons in the sample are analyzed, and this is assuming that no mineral-separation-induced biases are affecting the concentrated zircon fractions. It is important to note that intersample comparisons are commonly made by using results obtained with different types of mass spectrometers, lasers, and data reduction protocols conducted at different laboratories; this variability undoubtedly induces some degree analytical bias as recently shown by Košler et al. [17] in their results of a major inter-laboratory comparison experiment. This accuracy/precision induced variability is likely unavoidable until interlaboratory U-Pb age offsets are better understood and appropriately corrected for. This implies that the differences in age populations generated for Trials 1–4 include both sampling and analytical biases because three different grain mounts of CP40 were analyzed and two different LA-ICP-MS were used during the four trials.

5. **Handling Large-*n***

One major issue that has arisen during the creation and interpretation of large-*n* datasets is the inability to plot and evaluate the large quantities of data effectively, and at the same time address data quality. The most widely used program for plotting concordia diagrams, the Excel add-in *Isoplot* [55], can only plot 250 ellipses on a concordia diagram at the time, and only plots them in linear space. Likewise, the Java applet *DensityPlotter* [50] cannot plot more than 1000 analyses (at the time of this investigation) as histograms and KDE/PDP curves. In order to overcome this, we developed the in-house Python® codes *DensityDist* and *ConcordiaDraw*. These programs are fully capable of plotting publication-quality figures such as those shown in figures 4 and 5, and are unconstrained in terms of the number of analyses that can be handled at a time (however, they are limited by the floating memory of the computer used). *DensityDist* combines PDP and Gaussian KDE functions such as described in Vermeesch [50]. *ConcordiaDraw* is capable of plotting the traditional error ellipses at 68.3% and 95% confidence level, both in linear and logarithmic Wetherill concordia space. With large-*n* data, as *n* increases it becomes more difficult to evaluate individual error ellipses in a concordia diagram (Fig. 5A). Therefore, in addition to the traditional individual uncertainty ellipses, *ConcordiaDraw* also incorporates a density-contour mapping tool similar to that described by Sircombe [56] (Fig. 5B). These density-contour maps are available to be graphed in linear and logarithmic space. The latter offer a better way to visualize samples with a wide distribution of age ranges such as sample CP40 (Fig. 5B). Thus far, *ConcordiaDraw* only offers the possibility of density contouring using bivariate correlated PDP's, but in the future the capacity of performing this age mapping with KDE functions may also be implemented. It is expected that, as large-*n* datasets start to become more commonly applied within the geochronological community, there will be a joint effort towards continuing to improve the visualization and statistical tools we use to scrutinize and evaluate the data in the context of maximum depositional ages and interpretations of sedimentary provenance.

6. Future

In order to evaluate the power of large-*n* datasets, we conducted analyses on a sample with the *a-priori* knowledge that it would contain a wide spread of ages and a large number of age groups (CP40 from Dickinson and Gehrels[38]). This was done in order to investigate the possibility that conducting large-*n* analyses would generate results that arguably approach the 'true' age distribution of the sample. We anticipate that for many samples with small numbers of age fractions a value of *n* less than 1000 would be sufficient for complete sample characterization. For instance, in samples with unimodal age distributions, conducting more than 100 analyses would be unnecessary to address most geologic questions. Although the distribution and number of age fractions for a sample can be estimated by the geological setting of the unit under scrutiny, the ideal number analyses to run on an aliquot would remain uncertain until data are acquired and the number of age groups becomes more apparent. To that end, we suggest large-*n* is a not fixed number of analyses, but rather a range (*n*= 300–1000), depending on the number of age groups present. We anticipate that real-time data reduction (i.e., U-Pb ages generating continuously while data is being acquired with a mass spectrometer) will aid investigators in deciding when a sufficient number of observations have been reached. We envision a computer continuously reducing data (i.e., correcting for Pb/U fractionation, initial-Pb, instrument drift, and managing error propagation) as data are generated by the ICP-MS and then automatically populating *DensityDist* plots and *ConcordiaDraw* plots. This will allow investigators to observe: the PDP and KDE curves develop; low abundance age fractions reach critical thresholds (e.g., $n \geq 3$); and/or the youngest age cluster approach the 'true' depositional age of the rocks (if syn-depositional grains are present). This approach will allow investigators to use instrument time more efficiently and optimize strategies for solving geologic problems.

Critical for this approach to be viable is development of analytical methods that can generate U-Pb ages much more efficiently [22, 23]. Methods described herein allow generation of ages at a rate of 3–4 per minute depending on the instrument and acquisition routine (Table 1). This results in a total acquisition time, including laser targeting and preablation cleaning passes, of 3.5–7.0 hours for 1000 analyses. Given that these acquisition times are similar to acquisition of ~100 analyses using previous

methods (~4 hours), it is now feasible to generate much more robust datasets (n= 300–1000) at approximately the same cost as a traditional n= 100 dataset, and with minimal loss of precision/accuracy.

7. Conclusions

Large-n may enhance the geologic relevance of maximum depositional ages determined by the Principle of Inclusion. A larger number of ages for the young age component in an aliquot of a detrital sample, in some cases, may more closely approximate the 'true' deposition age of the rock.

The short acquisition times of total count U-Pb method using LA-ICP-MS coupled with the reasonably high precision and accuracy of this technique makes large-n provenance investigations a practical alternative to more traditional SIMS and LA-ICP-MS approaches.

Andersen [10] poised the question: "Is quantitative representation of the detrital zircon age distribution in a sediment possible for reasonable values of n (i.e., will observed age population abundances ever reflect those of the sediment)?" The large-n method described here addresses this question by establishing a methodology that redefines what a "reasonable" value of n means.

Large-n analysis allows detrital zircon provenance investigations to go beyond limiting the 'presence and absence of ages' approach, and use proportions of ages to address provenance questions in a more quantitative fashion.

Acknowledgements

This work was supported by the U.S. National Science Foundation (EAR-1032156, EAR-1338583, EAR-1118525, and AGS-1203427). We thank two anonymous reviewers for their clear and insightful reviews.

References

1. P.W. Reiners, I.H. Campbell, S. Nicolescu, C.M. Allen, J.K. Hourigan, J.I. Garver, J.M. Mattinson, and D.S. Cowan, *Am. J. Sci.*, 2005, **305**, 259-311.

2. M. Bernet and J.I Garver, in *Low-Temperature thermochronology: Techniques, Interpretations, and Applications*, eds. P.W. Reiners and T.A. Ehlers, Reviews in Mineralogy and Geochemistry Series, 2005, vol. 58, pp. 205-237.

3. B. Carrapa, P.G. DeCelles, P.W. Reiners, G.E. Gehrels, M. Sudo, *Geol.*, 2009, **237**, 407–410.

4. B. Carrapa, S. Bywater-Reyes, P.G. DeCelles, E. Mortimer and G.E. Geherels, *Basin Res.*, 2012, **24**, 249–268.

5. K. Hodges, K. Ruhl, C. Wobus, and M. Pringle, *Rev. Mineral. Geochemistry*, 2005, **58**, p. 239–257.

6. E. Enkelman, A. Weislogel, L. Ratschbacher, E. Edie, A. Renno and J. Wooden, 2007, *Tectonics*, **26**, doi:10.1029/2006TC002078.

7. G.E. Gehrels, 2000, *Geol. Soc. Am. Spec. Paper*, **347**, pp. 1–17.

8. G.E. Gehrels, in *Detrital Zircon U-Pb Geochronology*, ed. C. Busby and A. Azor, Wiley online, ISBN: 9781444347166, 2012.

9. C.M. Fedo, K.N. Sircombe and R.H. Rainbird, Zircon, in *Reviews in Mineralogy and Geochemistry*, ed. J. M. Hanchar and P. W. O. Hoskin, Mineralogical Society of America, Washington, DC, 2003, vol. 53, pp. 277–303.

10. T. Andersen, *Chem. Geol.*, 2005, **216**, 249–270.

11. L. Heaman, and R. Parrish, Heaman, L., and Parrish, R., in *Short course handbook on application of radiogenic isotope systems to problemns in geology*, ed. L. Heanman and J.N. Ludden, Mineralogical Association of Canada, 1991, pp. 59-102.

12. J.K.W. Lee, I.S. Williams and D.J. Ellis, 1997, *Nature*, **390**, 159–162.

13. B. Schoene, *Treatise on Geochemistry*, 2014, **4**, 341–378.

14. P. Vermeesch, *Earth Planet. Sci. Lett.*, 2004, **224**, 441–451.

15. G.E. Gehrels, V.A. Valencia and J. Ruiz, *Geochem., Geophys., Geosyst.*, 2008, **9**, doi:10.1029/2007GC001805.

16. L.A. Solari, A. Gómez-Tuena, J.P. Bernal, O. Pérez-Arvizu and M. Tanner, 2010, *Geostand. Geoanal. Res.*, **34**, 5–18.

17. J. Košler, J. Sláma, E. Belousova, F. Corfu, G.E. Gehrels, A. Gerdes, M.S.A. Horstwood, K.N. Sircombe, P.J. Sylvester, M. Tiepolo, M.J. Whitehouse and J.D. Woodhead, *Geostand. Geoanal. Res.*, 2013, **37**, 243–259.

18. S.A. Bowring, B. Schoene, J.L. Crowley, J. Ramezani and D.C. Condon, in *Geochronology: Emerging Opportunities Paleontological Society Papers*, ed. T. Olszewski, The Paleontological Society, Philadelphia, PA, 2006, vol. 12, pp. 25–45.

19. D.O. Froude, T.R. Ireland, P.D. Kinny, I.S. Williams, W. Compston, I.R. Williams and J.S Myers, *Nature*, 1983, **304**, 616–618.

20. M.H. Dodson, W. Compston, I.S. Williams and J.F. Wilson, *J. Geol. Soc. (London, U.K.)*, 1988, **145**, 997–983.

21. N. Machado and G. Gauthier, *Geochim. Cosmochim. Acta*, 1996, **60**, 5063–5073.

22. P. Holden, P. Lanc, T.R. Ireland, T.M. Harrison, J.J. Foster and Z. Bruce, *Int. J. Mass Spectrom.*, 2009, **286**, 53–63.

23. J.M. Cottle, A.R. Kylander-Clark and J.C. Vrijmoed, *Chem. Geol.*, 2012, **332-333**, 136–147.

24. J.M. Cottle, M.S.A. Horstwood and R.R. Parrish, J. Anal. At. Spectrom., 2009, **24**, 1355–1363.

25. S. Johnston, G. Gehrels, V. Valencia, J. Ruiz, *Chem. Geol.*, 2008, **259**, 218–229.

26. R.L. Lawrence, R. Cox, R.W. Mapes and D.S. Colemen, *Geol. Soc. Am. Bull.*, 2011, **123**, 295–305.

27. K.N. Sircombe and R.A. Stern, *Geochim. Cosmochim. Acta*, 2002, **66**, 2379–2397.

28. K.N. Sircombe, *Geochim. Cosmochim. Acta*, 2000, **64**, 1593–1616.

29. J.T. Jia, H.B. Zheng, T.X. Huang, F.Y. Wu, S.Y. Yang, K. Wang and M.Y. He, *Chin. Sci. Bull.*, 2010, **55**, 1520–1528.

30. W.H. Craddock and A.R.C. Kylander-Clark, *Geosphere*, 2013 **9**, 1832–1851.

31. A. Nemchin and P.A. Cawood, *Sediment. Geol.*, 2005, **182**, 143–162.

32. W. Compston, I.S. Williams and C. Meyer, *Geophys. Res. Suppl.*, 1984, **89**, B525–B534.

33. R.A. Sterns, and Y. Amelin, *Chem. Geol.*, 2003, **197**, 111–142.

34. L.A. Solari, A. Gómez-Tuena, J.P. Bernal, O. Pérez-Arvizu and M. Tanner, *Geostand. Geoanal. Res.*, 2009, **34**, 5–18.

35. W.R. Dickinson and G.E. Gehrels, *Geol. Soc. Am. Bull.*, 2009, **121**, 408–433.

36. P.G. DeCelles, G.E. Gehrels, Y. Najman, A.J. Martin, A. Carter, and E. Garzanti, *Earth and Plant. Sci. Lett.*, 2004, **227**, 313–330.

37. W.H. Amidon, D.W. Burbank, and G.E. Gehrels, *Earth Planet. Sci. Lett.*, 2005, **235**, 244–260.

38. W. Dickinson and G.E. Gehrels, *Am. J. Sci.*, 2008, **308,** 1041–1082.

39. G.E. Gehrels, V. Valencia and A. Pullen, 2006, in *Emerging Opportunities: Paleontology Society Papers,* ed. T. Olszewski, vol. 12, pp. 67–76.

40. G. Gehrels, M. Rusmore, G. Woodsworth, M. Crawford, C. Andronicos, L. Hollister, J. Patchett, M. Ducea, R. Butler, K. Klepeis, C. Davidson, B. Mahoney, R. Friedman, J. Haggart, W. Crawford, D. Pearson and J. Giradi, *Geol. Soc. Am. Bull.*, 2009, **121**, 1341–1361.

41. M.G. Malusá, A. Carter, M. Limoncelli, I.M. Villa and E. Garzanti, *Chem. Geol.*, 2013, **359**, 90–107.

42. L. Black, S. Kamo, C. Allen, D. Davis, J. Aleinikoff, J. Valley, R. Mundil, I. Campbell, R. Korsch, I. Williams and C. Foudoulis, *Chem. Geol.*, 2004, **205**, 115–140.

43. J.M. Mattinson, *Chem. Geol.*, 2010, **275**, 186–198.

44. J.B. Paces and J.D. Miller, *J. Geophys. Res.*, 1993, **98**, 13997–14013.

45. M. Wiedenbeck, P. Alle, F. Corfu, W.L. Griffin, M. Meier, F. Ober, A. von Quant, J.C. Roddick and J. Spiegel, *Geostand. Newsl.*, 1995, **19**, 1–23.

46. M.D. Schmitz and S.A. Bowring, *Geochim. Cosmochim. Acta*, 2003, **67**, 3665–3672.

47. R.F. Butler, G.E. Gehrels, S.L. Baldwin and C. Davidson, *J. Geophys. Res.*, 2002, **107,** EPM 3-1 to 3-13.

48. J. Sláma, J. Košler, D.J. Condon, J.L. Crowley, A. Gerdes, J.M. Hanchar, M.S.A. Horstwood and G.A. Morris, *Chem. Geol.*, 2008, **249**, 1–35.

49. D. Frei and A. Gerdes, 2009, *Chem. Geol.*, **261**, 261–270.

50. P. Vermeesch, *Chem. Geol.*, 2012, **312-313**, 190–194.

51. P. Vermeesch, *Chem. Geol.*, 2013, **341**, 140–146.

52. D.M. Pearson, P. Kapp, P.W. Reiners, G.E. Gehrels, M.N. Ducea, A. Pullen, J.E. Otamendi and R.N. Alonso, *Tectonics*, 2012, **31**, doi:10.1029/2011TC003043.

53. A.P. Willner, S. Sindern, R. Metzger, T. Ermolaeva, U. Kramm, V. Puchkov, and A. Kronz, *Precambrian Res.*, 2003, **124**, p. 1–20.

54. T. Andersen, *Geol. Mag.*, 2013, **150**, p. 426–440.

55. K.R., Ludwig, *Manual for Isoplot 3.7: Berkeley Geochrnology Center*, Special Publication No. 4, 2008, pp. 77.

56. K.N. Sircombe, *Geochem., Geophys., Geosyst.,* 2006, **7**, DOI: 10.1029/2005GC001052.

Figure Captions

Fig. 1: Histogram and kernel density estimation (KDE) plots of U-Pb zircon ages for CP40 from Gehrels and Dickinson (2008). The left-side shows the typical age information collected from a U-Pb detrital zircon ID-TIMS provenance study (*n*= 22), whereas the right-side shows the results from a typical (*n*= 100) LA-ICP-MS study.

Fig. 2: U-Pb zircon age offsets plots for Element2 (LA-SC-ICP-MS) and Nu Plasma (LA-MC-ICP-MS) versus published and unpublished TIMS U-Pb zircon ages [42–48]. $^{206}Pb/^{238}U$ ages and uncertainties (shown at 2σ) for LA-ICP-MS data from the weighted mean of 10–15 analyses.

Fig. 3: Cumulative age probability plots for Trials 1–4 and subsets of Trial 1. A) Cumulative age probability plots from Trials 1–4. B) Cumulative age probability plots from 10 subsets of *n*= 100 from Trial 1. C) Maximum range of cumulative age probability sets.

Fig. 4: Probability density plots (PDP), kernel density estimation plots (KDE), histograms, and age density (black crosses). A) Trial 1 show as 10 n=100 subsets. B) Trials 1–4 (n≈ 1000). C) Summation of Trials 1–4.

Fig. 5: Wetherill U-Pb concordia plots generated with *ConcordiaDraw* using ages< 2200 Ma from Trial 4 (n= 941). A) Traditional Wetherill concordia plot. B) Density contour concordia plot.

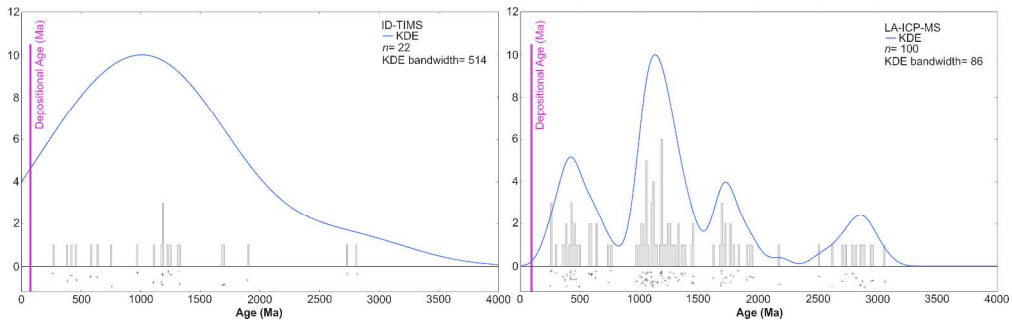

764x237mm (300 x 300 DPI)

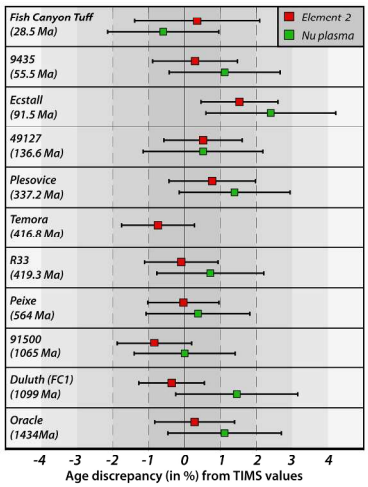

215x279mm (300 x 300 DPI)

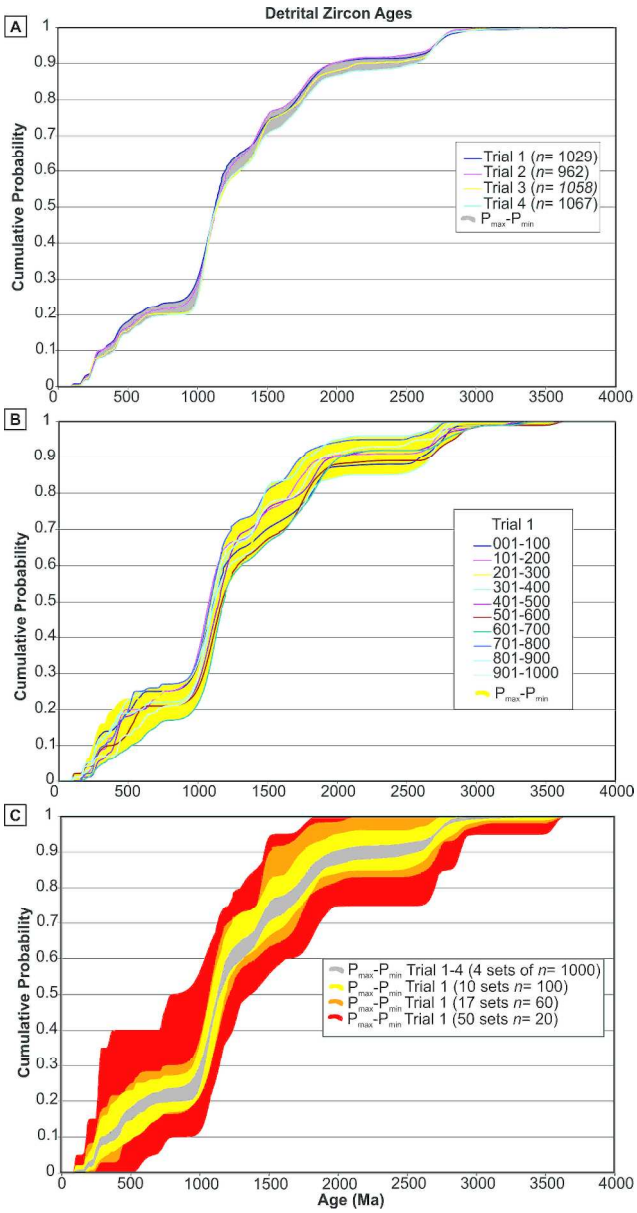

256x489mm (300 x 300 DPI)

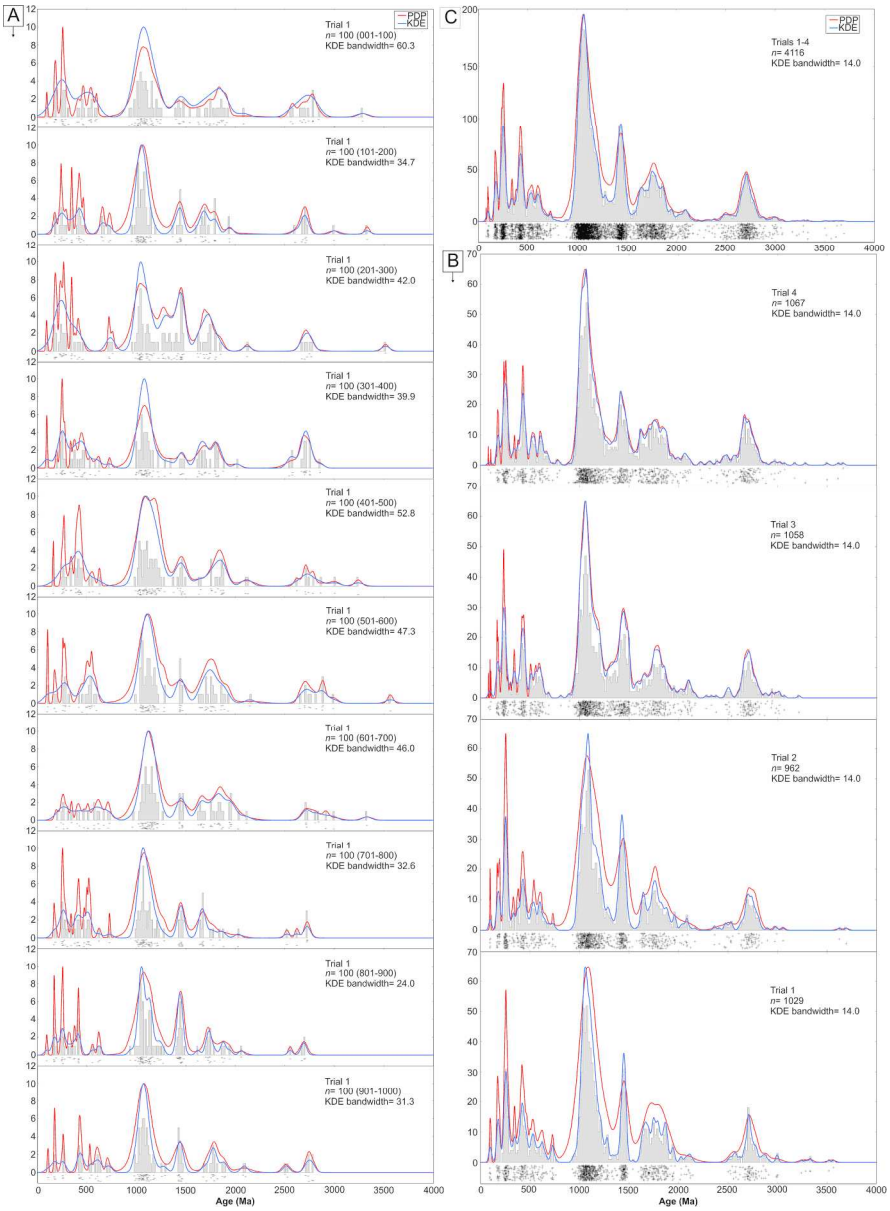

203x276mm (300 x 300 DPI)

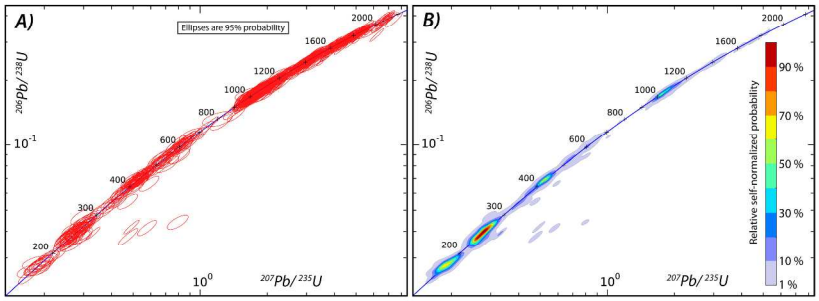

279x361mm (300 x 300 DPI)

Parameters	Nu: Total Counts Trial 1	Nu: Total Counts Trial 2	Element2: Total Counts Trials 3 and 4
Mass Spectrometer			
cool gas (L/min)	13.0	13.0	16.00
auxiliary gas (L/min)	0.80	0.80	0.80
sample/make-up gas (L/min)	1.06	1.06	1.323
power (W)	1300	1300	1250
supplemental N_2 (L/min)	N/A	N/A	< 0.100
Data Acquisition			
masses	Pb204, Pb206, Pb 207, Pb 208, Th232, U238	Pb204, Pb206, Pb 207, Pb 208, Th232, U238	Hg202, Pb204, Pb206, Pb 207, Th232, U238
detection mode	IC, IC, IC, IC, Faraday, Faraday	IC, IC, IC, IC, Faraday, Faraday	IC, IC, Both , Both , Both , Both
sample time per peak (s)	Simultaneous	Simultaneous	0.0010, 0.0010, 0.0150, 0.0200, 0.0010, 0.0040
number of samples per peak	N/A	N/A	4
total analyte sampling (s)	3	6	9
total time with backgrounds (s)	6	12	14
acquisition mode	Time Resolved Analysis	Time Resolved Analysis	sample blocks
acquisition initiation	laser scan	laser scan	external trigger from laser scan
Laser	Photon Analyte G2	Photon Analyte G2	Photon Analyte G2
type and wavelength	Excimer 193 nm	Excimer 193 nm	Excimer 193 nm
sample cell	Helex-Fast	Helex-Fast	Helex-Fast
constant energy set (mJ)	7.0	7.0	7.0
laser energy (%)	94	94	94
rep rate (Hz)	7	7	8
preablation pass	3 bursts at 25 µm	3 bursts at 25 µm	3 bursts at 50 µm
analysis pass	20 bursts at 12 µm	40 bursts at 12 µm	56 bursts at 30 µm
MFC1, MFC2 (L/min)	0.200, 0.050	0.200, 0.050	0.200, 0.080

IC= ion counting; Both = Automated selection of ion-counting or analog